JOURNAL OF GEOPHYSICAL RESEARCH: PLANETS, VOL. 118, 138–146, doi:10.1029/2012JE004274, 2013

The redox state, FeO content, and origin of sulfur-rich magmas on Mercury

Mikhail Yu. Zolotov,[1] Ann L. Sprague,[2] Steven A. Hauck II,[3] Larry R. Nittler,[4] Sean C. Solomon,[4,5] and Shoshana Z. Weider[4]

Received 3 October 2012; revised 29 November 2012; accepted 12 December 2012; published 31 January 2013.

[1] MErcury Surface, Space ENvironment, GEochemistry, and Ranging (MESSENGER) orbital observations of Mercury have revealed elevated S abundances, Ca-S and Mg-S correlations, and a low upper limit for ferrous iron in surface silicates. These data indicate the presence of Ca and/or Mg sulfides in volcanic rocks and a low oxygen fugacity (fO_2) in their parental magmas. We have evaluated coupled fO_2 and fS_2 values and FeO contents in Mercury's magmas from silicate-sulfide equilibria and empirical models for silicate melts and metallurgical slags. The evaluated fO_2 at 1700–1800 K is 4.5 to 7.3 $\log_{10}$ units below the iron-wüstite buffer. These values correspond to 0.028–0.79 wt % FeO, implying that Fe must be also present in sulfides and metal and are also consistent with the composition of the partial melt of an enstatite chondrite. This derived upper limit for FeO is substantially lower than the limits obtained from reflectance measurements of Mercury's surface materials. The low fO_2 and FeO values provide new constraints for igneous processes on Mercury as well as the formation, evolution, and internal structure of the innermost planet.

Citation: Zolotov, M. Yu., A. L. Sprague, S. A. Hauck II, L. R. Nittler, S. C. Solomon, and S. Z. Weider (2013), The redox state, FeO content, and origin of sulfur-rich magmas on Mercury, *J. Geophys. Res. Planets*, *118*, 138–146, doi:10.1029/2012JE004274.

1. Introduction

[2] Both telescopic and Mariner 10 observations of the spectral reflectance of Mercury indicate a low FeO content (< ~3–6 wt %) in surface silicates [e.g., *Vilas*, 1988; *Blewett et al*., 1997; *Robinson and Taylor*, 2001; *Boynton et al*., 2007; *Denevi and Robinson*, 2008]. Observations obtained by the MErcury Surface, Space ENvironment, GEochemistry, and Ranging (MESSENGER) spacecraft during its flybys of Mercury supported these results and indicated an upper limit on the FeO content in surface silicates of 2–4 wt % [*McClintock et al*., 2008]. The low upper limit for FeO is consistent with the low overall iron content of Mercury's surface (0.2–4.5 wt %, depending on location) subsequently determined from orbital measurements by MESSENGER's X-Ray Spectrometer (XRS) and Gamma-Ray Spectrometer (GRS) [*Nittler et al*., 2011; *Weider et al*., 2012; *Starr et al*., 2012; *Evans et al*., 2012].

[3] MESSENGER imaging and elemental remote sensing observations show that a substantial fraction of Mercury's surface consists of volcanic deposits [*Head et al*., 2009, 2012; *Weider et al*., 2012]. Therefore, the low FeO content in surface silicates could indicate unusually reduced (oxygen deficient) conditions in parental magmas and magma source regions in Mercury's mantle. The apparent shift of the $FeO = Fe^0 + 0.5\ O_2$ equilibrium toward Fe^0 metal signifies a low fugacity of oxygen (fO_2) in magmas on Mercury. The low FeO content in surface silicates also implies a strongly reduced composition for the materials from which Mercury accreted, indicating the presence of low-fO_2 environments in the inner portions of the solar nebula.

[4] Chemical and mineralogical characterization of enstatite chondrites [*Keil*, 1968], along with experimental data in chemical and metallurgical literature, indicates that low fO_2 can restrain the lithophile behavior of some elements (e.g., Mg, Ca, Ti, U, Th, Na, and K) and favor their bonding with S, if it is available. Therefore, speciation and concentration of these elements and S in Mercury's surface materials can be used to constrain the oxidation state of their parental magmatic systems [*Nittler et al*., 2011; *McCubbin et al*., 2012]. In turn, the behavior of elements in the interior of Mercury can be assessed if fO_2 values are known [e.g., *Malavergne et al*., 2010].

[5] The low FeO content in Mercury's silicates is consistent with the unusually high S concentrations (~1–6 wt %) in surface materials detected by MESSENGER XRS and

[1]School of Earth and Space Exploration, Arizona State University, Tempe, Arizona, USA.
[2]Lunar and Planetary Laboratory, University of Arizona, Tucson, Arizona, USA.
[3]Department of Earth, Environmental, and Planetary Sciences, Case Western Reserve University, Cleveland, Ohio, USA.
[4]Department of Terrestrial Magnetism, Carnegie Institution of Washington, Washington, D.C., USA.
[5]Lamont-Doherty Earth Observatory, Columbia University, Palisades, New York, USA.

Corresponding author: A. L. Sprague, Lunar and Planetary Laboratory, University of Arizona, Tucson, Arizona 85721, USA. sprague@lpl.arizona.edu

2169-9097/13/2012JE004274

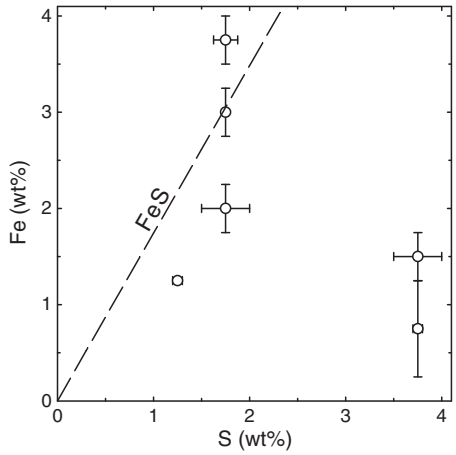

Figure 1. Concentrations of S and Fe in Mercury surface materials detected with MESSENGER XRS [*Nittler et al*., 2011], obtained for an assumed Si abundance of 25 wt %. The dashed line corresponds to the Fe/S weight ratio in troilite. Other XRS data [*Weider et al*., 2012] provide some support for the Fe-S correlation along the FeS line. Note that the two data points well removed from the trend are repeated measurements of a single region, which may be an outlier.

GRS instruments [*Nittler et al*., 2011; *Weider et al*., 2012; *Starr et al*., 2012; *Evans et al*., 2012]. The high S content could reflect the anomalously high (up to ~10 wt %) solubility of sulfide S at fO_2 values more than 2 $\log_{10}$ units below that for the iron-wüstite (IW, Fe-$Fe_{0.947}O$) buffer ($fO_2 <$ IW-2) [e.g., *Richardson and Fincham*, 1954; *Fogel et al*., 1996; *McCoy et al*., 1999; *Berthet et al*., 2009]. These experimental data show that the high solubility of S in silicate/oxide melts is mainly caused by the association of S with Ca, Mg, and Fe, which behave as lithophile elements at more oxidized conditions. Indeed, positive correlations between Ca and S and between Mg and S in surface materials on Mercury suggest the presence of Ca and Mg sulfides [*Nittler et al*., 2011; *Weider et al*., 2012], which are common in enstatite chondrites [*Keil*, 1968; *Brearley and Jones*, 1998]. These chondrites are often considered among the analogs of Mercury's precursory materials because they are rich in the FeO-poor Mg silicate enstatite and their partial melts are similar in composition to Mercury's surface materials as measured by MESSENGER XRS data [*Wasson*, 1988; *Burbine et al*., 2002; *Taylor and Scott*, 2003; *Nittler et al*., 2011]. The weak absorption feature at 0.6 μm reported for some high-albedo younger areas on Mercury is consistent with the presence of Mg and/or Mn sulfides [*Vilas et al*., 2012]. A possible correlation between S and Fe seen in XRS data (Figure 1) and some interpretations of Mercury's reflectance spectra [*Vernazza et al*., 2010; *Blewett et al*., 2013] both suggest the presence of troilite (FeS) in surface materials. These observations agree with an earlier prediction of sulfides at Mercury's surface [*Sprague et al*., 1995]. By analogy with enstatite chondrites, sulfides containing Ni, Cr, Ti, K, and Na may also be present.

[6] Abundant experimental data and theoretical deductions for the metal-oxide and sulfide-oxide equilibria show that the concentration of FeO in silicate/oxide melts depends on fO_2 [e.g., *Roeder*, 1974; *Ariskin et al*., 1993; *Liu et al*., 2001; *O'Neill and Eggins*, 2002; *Wade et al*., 2012], and the concentration (solubility) of S in these melts is affected by both fO_2 and fS_2 [e.g., *Richardson and Fincham*, 1954; *Nzotta et al*., 1999; *Shankar et al*., 2006; *Taniguchi et al*., 2009]. These dependencies are also functions of melt composition and temperature. Therefore, the possible high abundance of sulfides and the low FeO content of surface silicates constrain the petrology and redox state of Mercury's magmas and igneous rocks. Here we present an evaluation of the fugacity of O_2 and S_2 and the corresponding FeO contents in typical magmas on Mercury. In particular, we have determined upper limits on fO_2 from reported upper limits on FeO in surface silicates. From concentrations of S obtained by MESSENGER measurements, we evaluated fO_2 on the basis of data from metallurgical slags. From the fO_2 values so inferred, we have constrained the FeO contents of magmas and volcanic rocks. We also discuss here the implications of these results for igneous processes on Mercury and the formation, evolution, and internal structure of the planet.

2. Fugacities of S_2 and O_2, and FeO and S Contents of Magmas on Mercury

2.1. Approaches

[7] We have made use of several independent methods to evaluate fS_2, fO_2, and FeO contents in magmas on Mercury. We have considered thermochemical equilibria of sulfides with metals, oxides, and silicates. The values of fO_2 and fS_2 were evaluated from equilibrium constants of corresponding reactions and assumed activities of chemical species. In addition, we used empirical dependencies inferred from petrologic experiments and the literature on metallurgical slags that connect the FeO concentration with fO_2 and the S content with fS_2 and fO_2 in silicate/oxide melts saturated with respect to Fe^0 metal. These numerical dependencies are functions of melt composition and temperature but not the activities of species. All evaluations have been based on the assumption that the chemical and mineralogical compositions of Mercury's surface materials inferred from spacecraft measurements correspond to the characteristics of the planet's igneous rocks and their parental melts.

[8] The fugacity of S_2 is a fundamental parameter related to the speciation and concentration of sulfur in melts. It is linked to the redox state (fO_2) because these two fugacities control the partitioning of metals between sulfide and oxide species, as discussed below. Because fS_2 values have not been measured experimentally for reduced silicate magmas, we have evaluated fS_2 from the equilibrium constants of metal-sulfide equilibria

$$2\ \mathrm{MS} = 2\ \mathrm{M} + \mathrm{S}_2(g), \tag{1}$$

where M is a metal (section 2.2). Our assumption is that fS_2 values in Mercury's melts do not exceed fS_2 in equilibrium with the least stable metal sulfide. The estimated upper limits on fS_2 have been further applied to constrain fO_2 from coupled fO_2-fS_2 relations (sections 2.4 and 2.5).

[9] The upper limits on the FeO content of surface silicates obtained from spectral reflectance observations of surface materials [e.g., *McClintock et al*., 2008] were used to evaluate upper limits on fO_2 in corresponding magmas (section 2.3). This evaluation was made with the empirical approach of

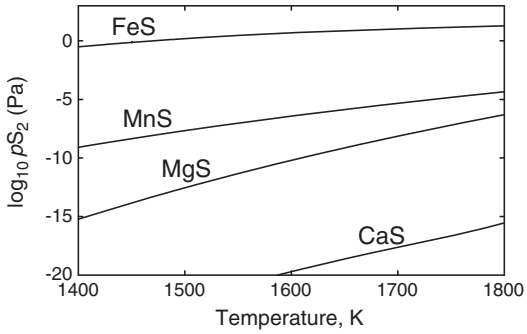

Figure 2. Partial pressure (p) of S_2 in equilibrium with sulfides at 0.1 MPa. The data refer to equilibrium as expressed in equation (1), where M is metal and MS and M are condensed phases with unity activities. The pS_2 values are identical to fS_2. The data correspond to equilibrium constants calculated at a standard pressure of 0.1 MPa from thermodynamic data of *Pankratz et al.* [1987] and *Robie and Hemingway* [1995]. The FeS data also represent the pS_2 in the Fe-FeS system [*Guillermet et al.*, 1981]. The data show the lower stability of FeS than for other sulfides.

Ariskin et al. [1993] that links fO_2, FeO molar content, and the silicate composition of Fe^0-saturated silicate melts. Although this method is based on a fit of experimental data for S-depleted melts, it does not consider the activities of FeO and Fe^0 in melts and leads to fO_2 evaluations comparable with those from other approaches [e.g., *McCubbin et al.*, 2012].

[10] The fugacities of O_2 and S_2 are linked through oxide-sulfide equilibria in reduced melts, as exemplified by the following equilibrium and its equilibrium constant:

$$\mathrm{MgO(melt)} + 0.5\ \mathrm{S_2} = \mathrm{MgS(melt)} + 0.5\ \mathrm{O_2} \qquad (2)$$

$$K_2 = \frac{a_{\mathrm{MgS}}\, f\mathrm{O_2}^{0.5}}{a_{\mathrm{MgO}}\, f\mathrm{S_2}^{0.5}}$$

where a denotes activity. We calculated the equilibrium constants of several oxide-sulfide equilibria to evaluate the dependencies of coupled fO_2 and fS_2 on the activities of oxides and sulfides. In addition, the assumed presence of some crystalline silicates in magmas permits the consideration of silicate-sulfide equilibria. In such cases, the activities of oxides are controlled by the coexisting silicates, and coupled fS_2-fO_2 relations are functions of sulfide activity and temperature. Therefore, we evaluated fS_2-fO_2 relations in melts from silicate-sulfide equilibria for appropriate sulfide activities and temperatures (section 2.4).

[11] Another approach for estimating the relationship between fO_2 and fS_2 is to use empirical data on the sulfide capacity (C_S) of metallurgical slags, defined as

$$C_S = (\mathrm{S}\%)\frac{f\mathrm{O_2}^{0.5}}{f\mathrm{S_2}^{0.5}}, \qquad (3)$$

where S% is the wt % of S in a slag [*Richardson and Fincham*, 1954]. In other words, sulfide capacity is a constant in the equation that connects S solubility in Fe^0-metal-saturated oxide melts (slags) with fO_2 and fS_2. The composition and temperature dependence of C_S has been determined from numerous experiments at controlled fS_2-fO_2 conditions and can be calculated with published empirical models [e.g., *Taniguchi et al.*, 2009]. Many of these models require the knowledge of optical basicity [*Duffy*, 1996], which depends on the oxide composition of the melt and reflects its acid-base properties. C_S strongly correlates with optical basicities of slags [*Shankar et al.*, 2006]. We evaluated optical basicities and sulfide capacities of melt compositions for Mercury, and we calculated coupled fS_2-fO_2 relations for appropriate temperatures with equation (3) (section 2.5). The results have been compared with fS_2-fO_2 data obtained from silicate-sulfide equilibria (section 2.4).

[12] The fO_2 values in melts were then estimated from coupled fS_2-fO_2 values and fS_2 constrained from equilibrium, expressed as in equation (1). Finally, the FeO content in magmas and igneous rocks was evaluated from the FeO-fO_2 relations inferred for melts on Mercury after *Ariskin et al.* [1993] (section 2.6).

[13] The evaluations of fO_2, fS_2, and FeO contents were performed at 1600–1800 K. The temperature of 1800 K is close to the estimated liquidus temperature for Mercury's silicate melts [*Stockstill-Cahill et al.*, 2012]. At 1600–1700 K, crystalline Mg silicates may coexist with silicate and immiscible sulfide melts, as inferred from melting experiments with the Indarch (EH4) enstatite chondrite (EC) [*McCoy et al.*, 1999]. Partial melts of enstatite chondrites are widely considered as analogs of magmas on Mercury [e.g., *Burbine et al.*, 2002; *Nittler et al.*, 2011; *Stockstill-Cahill et al.*, 2012]. Therefore, this temperature range is appropriate for evaluations of coupled fS_2 and fO_2 from silicate-sulfide equilibria. The majority of the metallurgical data used here are for temperatures at and above ~1700 K. Therefore, temperatures between 1700 and 1800 K are most suitable for the evaluation of fS_2 and fO_2 from metallurgical slag data. Our evaluations obtained from different approaches are compared at 1700 K.

2.2. Constraints on fS_2 in Magma

[14] The high S content in Mercury's rocks implies a high solubility of S in silicate melts. Some magmatic S could occur in immiscible sulfide liquids, as observed in partial melts of the Indarch EC at temperatures less than 1700 K [*McCoy et al.*, 1999]. The fS_2 of Mercury's magmas could be controlled by equilibria of dissolved and/or immiscible sulfides with S_2-dominated gas. The less stable sulfide species would disproportionally contribute to the value of fS_2. The stability of metal sulfides increases in the order Fe, Mn, Mg, and finally Ca. This sequence is seen in the decreasing equilibrium partial pressure (p) of S_2 in sulfide evaporation reactions at 1700 K (FeS, 10.6 Pa; MnS, $10^{-5.3}$ Pa; MgS, $10^{-8.1}$ Pa; CaS, $10^{-17.6}$ Pa) and is also illustrated in Figure 2. FeS, as the least stable sulfide, would have a relatively large effect on fS_2, and the fS_2 value for the FeS-Fe melt sets an upper limit for silicate melts on Mercury. However, the presence of coexisting sulfide and Fe-metal melts in EC melting experiments [*McCoy et al.*, 1999] together with a Fe-S correlation in Mercury surface materials (Figure 1) imply fS_2 values near the Fe-FeS melt equilibrium.

2.3. The fO_2 in Magma from Upper Limits on the FeO Content of Surface Silicates

[15] The empirical equation of *Ariskin et al.* [1993] was used to calculate the fO_2 values as a function of the FeO

Table 1. Sulfur-free Composition and Sulfur Content (wt%) of Mercury and a Possible Analog Composition[a]

	Northern Volcanic Plains	Intercrater Plains and Heavily Cratered Terrain	Indarch 1700 K melt
SiO_2	58.9	54.9	59.3
TiO_2	0.92	0.86	0.24
Al_2O_3	15.4	12.8	15.2
FeO	3.54	3.30	0.28
MnO	0.71	0.66	0.13
MgO	14.9	20.9	15.4
CaO	4.40	5.63	11.4
Na_2O	0.24	0.12	0.00
K_2O	0.21	0.10	0.00
S	1.5	2.3	4.36

[a]All three S-free compositions are from *Stockstill-Cahill et al.* [2012]; the first two are derived from MESSENGER XRS data [*Nittler et al.*, 2011; *Weider et al.*, 2012], and the third is from melting experiments by *McCoy et al.* [1999]. All Fe is assumed to be in FeO. Average concentrations of S in Mercury surface materials and Indarch melt are from *Weider et al.* [2012] and *McCoy et al.* [1999], respectively.

Table 2. Oxygen Fugacity ($\log_{10}$ Values Below the IW Buffer) and FeO Content in Possible Silicate Melts on Mercury[a]

	1600 K	1700 K	1800 K
$\log_{10} fO_2$ at IW	−10.5	−9.5	−8.7
pS_2 at Fe-FeS (Pa)	4.9	10.6	18.8
$\log_{10} fO_2$ from FeO Abundances			
< 4 wt% FeO	<IW-2.93	<IW-3.05	<IW-3.10
< 2.6 wt% FeO	<IW-3.30	<IW-3.45	<IW-3.50
0.25 wt% FeO	–	IW-5.2	–
fO_2 and FeO from equation (5) at $a_{MgS} = 0.6$ and the Fe-FeS S_2 Buffer			
fO_2	IW-5.9	IW-5.6	IW-5.4
FeO (mol%)	0.10	0.17	0.23
FeO (wt%)	0.12	0.21	0.28
fO_2 and FeO from C_S of Melts at the Fe-FeS S_2 Buffer			
fO_2 for NVP, 1.5 wt% S	IW-6.4 ± 0.5	IW-6.0 ± 0.4	IW-5.8 ± 0.5
fO_2 for IcP-HCT, 2.3 wt% S	IW-6.1 ± 0.3	IW-5.7 ± 0.3	IW-5.6 ± 0.5
FeO (wt%) for NVP	0.04–0.14	0.07–0.22	0.10–0.32
FeO (wt%) for IcP-HCT	0.06–0.15	0.13–0.25	0.13–0.44

[a]The fO_2 data at IW represent iron-wüstite equilibrium at 0.1 MPa calculated from thermodynamic data [*Robie and Hemingway*, 1995]. The fS_2 data for Fe-FeS melt are from *Guillermet et al.* [1981]. The fO_2 values are calculated from observational upper limits on FeO contents in Mercury surface materials and from the FeO abundance (0.25 wt%) in a partial melt of the Indarch enstatite chondrite. The calculations were performed with the approach of *Ariskin et al.* [1993] and are depicted in Figure 3. The FeO contents evaluated from equation (5) for that approach are for the S-free compositions for northern volcanic plains (NVP) and intercrater plains and heavily cratered terrain (IcP-HCT) (Table 1). The fO_2 values evaluated from sulfide capacities of compositions NVP and IcP-HCT (Table 1) are shown in Figures 4 and 5 for fS_2 at the Fe-FeS buffer. The corresponding FeO contents evaluated from FeO-fO_2 relationships can be seen in Figure 3.

content for silicate compositions that might represent Mercury's magmas, following *Stockstill-Cahill et al.* [2012] (Table 1). Two compositions represent the northern volcanic plains (NVP) and a mix of intercrater plains and heavily cratered terrain (IcP-HCT), and a third S-free composition is a normalized partial melt of the Indarch EC. All three compositions led to similar coupled fO_2-FeO values calculated at temperatures of 1600–1800 K (Figure 3). These data allowed us to estimate fO_2 from FeO abundances and vice versa (Table 2).

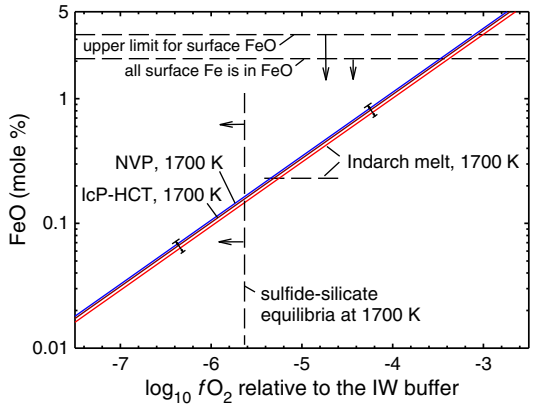

Figure 3. Relations among fO_2 and FeO content at 1700 K for the metal-saturated compositions shown in Table 1. The relations are calculated from the empirical equation of *Ariskin et al.* [1993]. The brackets refer to fO_2-FeO values for those compositions for temperatures of 1600–1800 K; higher FeO content corresponds to higher temperature. The horizontal dashed lines indicate upper limits for the FeO abundance in Mercury surface materials (4 wt% [*McClintock et al.*, 2008]; 2.6 +wt% [e.g., *Evans et al.*, 2012]) and for the FeO content in the Indarch partial melt at 1700 K [*McCoy et al.*, 1999]. The vertical dashed line shows fO_2 evaluated from equation (5) for fS_2 at the Fe-FeS buffer (see Figure 4a). The intersection of this line with the fO_2-FeO lines gives an upper limit on the FeO content in magmas.

[16] For the upper limit of 4 wt% FeO in surface silicates [*McClintock et al.*, 2008], the evaluated fO_2 value is IW-2.9 to IW-3.1 (Figure 3). If all Fe in surface materials (0.2–4.5 wt%) [*Nittler et al.*, 2011; *Evans et al.*, 2012; *Starr et al.*, 2012; *Weider et al.*, 2012] occurs in ferrous silicates, the evaluated values are IW-3.3 to IW-3.5 for an average of 2 wt% Fe (2.6 wt% and ~2.1 mol% FeO). For a partial melt of the Indarch enstatite chondrite with 0.25 wt% FeO [*McCoy et al.*, 1999], the evaluated fO_2 value is IW-5.2. The same value is obtained for the lowest value of 0.19 wt% Fe (0.24 wt% FeO) reported from MESSENGER electron-induced X-ray fluorescence data [*Starr et al.*, 2012].

2.4. Coupled fS_2 and fO_2 from Silicate-Sulfide Equilibria

[17] The melting experiments with the Indarch EC sample reveal that crystals of the Mg silicates enstatite (En, $Mg_2Si_2O_6$) and forsterite (Fo, Mg_2SiO_4) coexist with silicate and sulfide melts [*McCoy et al.*, 1999]. The mid-infrared spectral features for Mg silicates on Mercury (see *Boynton et al.* [2007] for a review), the Mg-rich composition of surface materials, and the observed Mg-S correlation [*Nittler et al.*, 2011; *Weider et al.*, 2012] imply similar occurrences in Mercury's magmas. We thus assume that fS_2 and fO_2 in the magmas are linked in silicate-sulfide equilibrium, so that

$$Mg_2SiO_4(\text{solid}) + 0.5\ S_2 = MgS(\text{melt}) + 0.5\ Mg_2Si_2O_6(\text{solid}) + 0.5\ O_2. \quad (4)$$

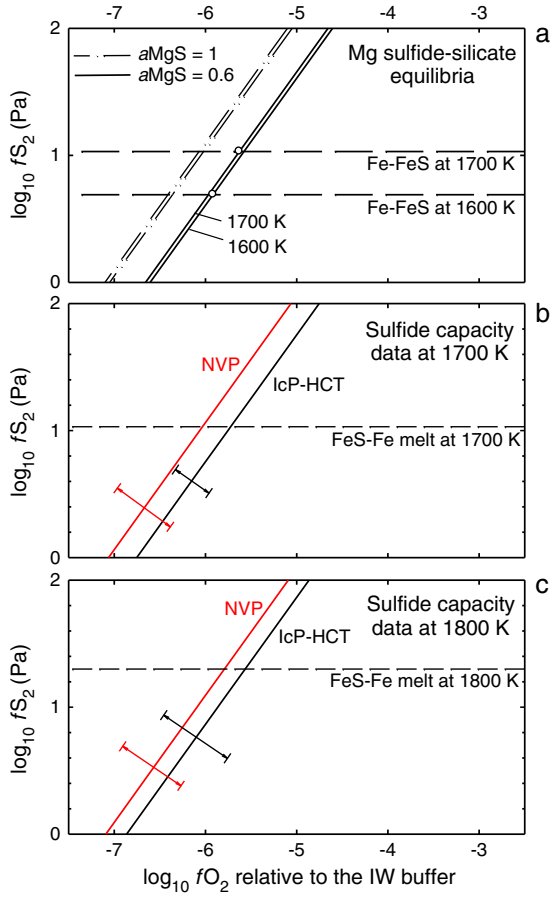

Figure 4. Relations among fO_2 and fS_2 for silicate melts on Mercury. (a) The fO_2 and fS_2 values are set by equilibrium expressed by equations (4) and (5) at two values for the activity of MgS. The dashed lines correspond to the fS_2 values in the Fe-FeS system [*Guillermet et al.*, 1981]. fS_2 may not exceed these values in magmas on Mercury (see text). The intersections of the silicate-sulfide equilibrium lines with fS_2 lines (open circles) set the fO_2 values shown in Table 2. (b and c) Relations between fO_2 and fS_2 in Mercury melts evaluated with equation (3) and with the S contents and C_S values shown in Tables 1 and 3. Brackets denote statistical uncertainties in the calculated values. The intersections of the inclined lines with the horizontal fS_2 lines for the Fe-FeS system determine fO_2 values (see Table 2).

[18] The fugacities fS_2 and fO_2 are variables in the expression for the equilibrium constant

$$K_4 = \frac{a_{MgS}\, a_{En}^{0.5} fO_2^{0.5}}{a_{Fo} fS_2^{0.5}} \quad (5)$$

where a denotes the activity of a solid species. Figure 4a shows the fO_2-fS_2 conditions for equilibrium (4) with K_4 calculated from standard thermodynamic properties (at 0.1 MPa) of the respective species [*Pankratz et al.*, 1987; *Robie and Hemingway*, 1995]. The activity of the silicates was assumed to be unity, reflecting the presence of FeO-poor Mg silicates observed in mid-infrared spectra of Mercury [*Boynton et al.*, 2007; *Sprague et al.*, 2009] and in the products of EC melting experiments [*McCoy et al.*, 1999]. The activity of MgS was varied from unity for the pure condensed species to 0.6 for admixtures of FeS and MnS observed in chondritic (EH3) niningerite. Because the enstatite-forsterite coexistence (0.5 En + MgO = Fo) determines aMgO in the melt (0.21 at 1700 K), identical results were obtained for the oxide-sulfide equilibrium given by equation (2).

[19] Lower temperatures and analogous considerations for Ca and Mn silicate-sulfide equilibria lead to lower fO_2 values. An admixture of Ca or Mn into pyroxene would lead to lower fO_2 than for pure enstatite. It follows that the evaluations for equilibria in equations (4) and (2) set an upper limit to fO_2 at a specified fS_2 value. At the value for fS_2 in equilibrium with the Fe-FeS melt [*Guillermet et al.*, 1981], the fO_2 value is IW-5.6 at 1700 K (Figure 4a, Table 2). Analogous evaluations at 1800 K make less sense because of a lack of crystalline silicates and/or immiscible sulfide liquids at near-liquidus conditions [*McCoy et al.*, 1999; *Stockstill-Cahill et al.*, 2012].

2.5. Coupled fS_2 and fO_2 from Sulfide Capacity Data

[20] Although magma-like compositions have not been explored in multiple metallurgical slag experiments, we have obtained consistent sulfide capacity (C_S) values for Mercury's melts from five empirical models [*Sosinsky and Sommerville*, 1986; *Young et al.*, 1992; *Nzotta et al.*, 1999; *Shankar et al.*, 2006; *Taniguchi et al.*, 2009] (Table 3). With each of these models, C_S was calculated as a function of melt composition and temperature. The lack of experimental data on C_S for magma-like compositions could in part account for the diversity of calculated C_S values.

[21] The fS_2-fO_2-S% relations calculated with equation (3) for C_S data averaged for the five models (Table 3) are shown in Figures 4b, 4c, and 5. The relations are slightly different for the NVP and IcP-HCT compositions, whereas the results for the Indarch partial melt composition are similar to those for the IcP-HCT composition. At an fS_2 value appropriate to the Fe-FeS buffer, the evaluated fO_2 values for NVP and IcP-HCT are in good agreement with those obtained for equilibrium as expressed in equation (5) (Table 2). However, the use of high Na_2O (4 wt %) abundances for NVP and IcP-HCT compositions [*Evans et al.*, 2012] leads to more oxidized fO_2 values, higher by 0.6 and 0.4 log units, respectively. The fO_2 value obtained for the Indarch melt (IW-6.2 ± 0.56 at 1700 K) agrees with the value of IW-5.9 evaluated by *Malavergne et al.* [2010] for the data of *McCoy et al.* [1999] for 1773 K melt.

[22] The coupled S%-fO_2 relations obtained from C_S data for Mercury's NVP and IcP-HCT compositions are not in complete agreement with petrologic experiments on S solubility [*McCoy et al.*, 1999; *Malavergne et al.*, 2007a; *Berthet et al.*, 2009] (Figure 5). Most of the experimental data indicate higher fO_2 for a given S abundance. This discrepancy may reflect a range of temperature and pressure conditions and melt compositions, a systematic discrepancy in calculations of C_S from slag models applied to magmatic compositions which differ from typical slags, uncertain fS_2 conditions in petrologic experiments, and the adopted fS_2 value in our calculations. Formally, the petrologic data could be matched within the framework of the slag C_S model if the experimental value of fS_2 were higher than at the Fe-FeS buffer. Comparison of our results with petrologic data, however, shows that fS_2 in EC melts and magmas on Mercury cannot be less than that at Fe-FeS

Table 3. Optical Basicity (Λ) and Sulfur Capacity ($\log_{10} C_S$) of Mercury and a Possible Analog Composition[a]

C_S Model	Northern Volcanic Plains ($\Lambda = 0.564$)			Intercrater Plains and Heavily Cratered Terrain ($\Lambda = 0.580$)			Indarch Melt ($\Lambda = 0.573$)
	1600 K	1700 K	1800 K	1600 K	1700 K	1800 K	1700 K
SS86	−5.69	−5.39	−5.12	−5.54	−5.21	−4.91	−5.28
YO92	−6.30	−5.87	−5.49	−5.91	−5.48	−5.10	−5.73
NZ99	−6.38	−5.75	−5.18	−5.94	−5.30	−4.73	−5.02
SH06	–	−5.31	−4.89	–	−5.06	−4.63	−5.16
TA09	−6.05	−5.78	−5.54	−5.76	−5.34	−5.34	−4.99
	-6.1 ± 0.27	-5.6 ± 0.22	-5.24 ± 0.24	-5.79 ± 0.16	-5.28 ± 0.14	-4.49 ± 0.26	-5.24 ± 0.28

[a]Optical basicity and C_S data correspond to S-free compositions of silicate melts (Table 1). Optical basicities were calculated after *Duffy* [1996] and used to calculate C_S for five independent models for metallurgical slags. The uncertainties given for average C_S reflect the differences in values obtained from the five models. SS86, *Sosinsky and Sommerville* [1986]; YO92, *Young et al.* [1992]; NZ99, *Nzotta et al.* [1999]; SH06, *Shankar et al.* [2006]; TA09, *Taniguchi et al.* [2009].

equilibrium. By this comparison, our fO_2 values are appropriate estimates rather than upper limits. The lack of information on fS_2 in petrologic experiments, however, limits the strength of this argument. Further experiments on S solubility in magma-like melts at fixed fS_2 and fO_2 will help to reconcile the discrepancy noted here and will further constrain the redox state of magmas on Mercury.

2.6. FeO Content in Melts and Igneous Rocks

[23] The concentration of FeO in partial melts and corresponding igneous rocks has been evaluated from the FeO-fO_2 relations established for Mercury's surface compositions with the approach of *Ariskin et al.* [1993] (Figure 3). The evaluated fO_2 range of IW-6.4 to IW-5.1 for NVP and IcP-HCT compositions with 1.5 and 2.3 wt % S, respectively, corresponds to 0.07–0.44 wt % FeO in melts at 1700–1800 K (Table 2). These evaluated FeO contents are close to the 0.25 wt % FeO reported for partial melt of Indarch at 1700 K [*McCoy et al.*, 1999]. The match of the calculated and experimental FeO values provides some validation of our numerical approaches. Therefore, the fO_2 values of ~IW-5 and 0.44 wt % FeO are taken to be upper limits that supersede other evaluations presented in Table 2.

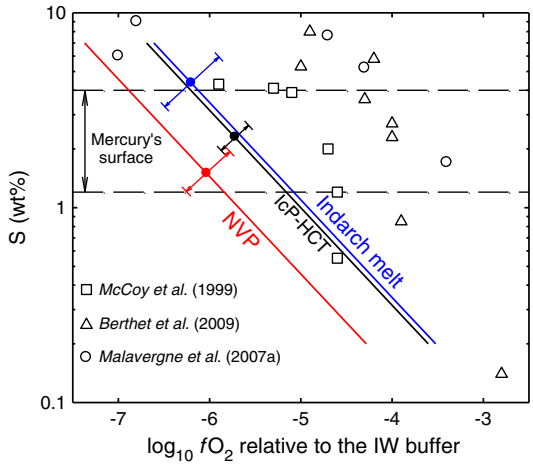

Figure 5. The solubility of S in reduced silicate melts as a function of fO_2. The solid lines show the values evaluated from sulfide capacities of melts (Table 3) at fS_2 controlled by Fe-FeS melt equilibrium at 1700 K (Table 2). The uncertainties reflect the range of C_S values. The solid symbols show fO_2 at S contents depicted in Table 1. The open symbols show petrologic experimental data performed at different temperatures, pressures, and melt compositions. Note that fS_2 is not specified for these experiments. The dashed lines show the range of S concentrations in surface materials on Mercury [*Nittler et al.*, 2011]. These data determine fO_2 for the range of S contents in Mercury materials (Table 2).

[24] For a range of S abundances on Mercury of 1.2–4 wt % and with fS_2 at the Fe-FeS buffer, the evaluated fO_2 value is between IW-4.5 and IW-7.3 at 1700–1800 K, including uncertainties in C_S (Figure 5). These fO_2 values correspond to FeO concentrations of 0.028–0.79 wt % (~0.023–0.65 mol %) in melts and igneous rocks. This range reflects variations in silicate composition, S content, and uncertainties in the data.

3. Implications of Low fO_2 and High S Content in Mercury's Surface Material

[25] The upper limits on fO_2 obtained above confirm earlier inferences [e.g., *Robinson and Taylor*, 2001; *Nittler et al.*, 2011; *McCubbin et al.*, 2012] about strongly reducing conditions in Mercury's igneous systems. The derived low concentration of FeO in silicates is less than upper limits evaluated from spectral reflectance measurements [e.g., *Vilas*, 1988]. The evaluated concentration of FeO in silicates is generally lower than the Fe concentrations reported from XRS [*Nittler et al.*, 2011; *Weider et al.*, 2012] and GRS data [*Evans et al.*, 2012]. Therefore, Fe must also be present as troilite, as an FeS admixture in Mg-rich sulfides, and possibly in the metallic form. Both metal and sulfides could have separated and crystallized from cooling magma at near-surface conditions [cf. *McCoy et al.*, 1999]. The low fO_2 values exclude ilmenite ($FeTiO_3$) as a major darkening surface mineral [cf. *Riner et al.*, 2010; *Zolotov*, 2011].

[26] The strong effect of fO_2 on S solubility at fugacities less than ~IW-2.5 implies that the variable S content observed on Mercury may reflect redox heterogeneity of the igneous systems on the planet. However, evaluations from C_S data show that although the IcP-HCT regions are relatively enriched in S, Mg, and Ca, they may not be more reduced than the NVP areas (Figures 4b, 4c, and 5 and Table 2). The solubility of S at $fO_2 <$ IW-1 could increase with temperature [*Malavergne et al.*, 2012], and the high temperatures implied by the Mg-rich IcP-HCT melts (Table 1) may have contributed to the elevated S contents. Higher S concentrations may also reflect efficient assimilation of crustal S-bearing minerals by high-temperature melts, as observed in komatiites [*Bekker et al.*, 2009]. Condensation of S-bearing species emitted from hot lavas with mantle or assimilated S may also play a role.

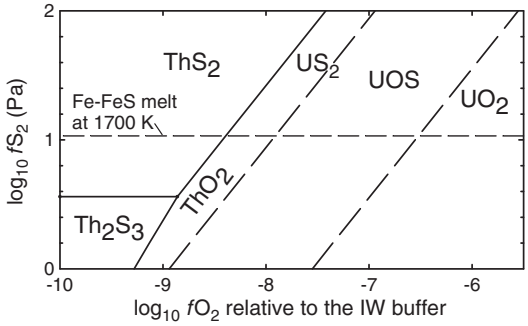

Figure 6. Stability fields of U and Th sulfides at 1700 K and 0.1 MPa. The phase boundaries of U and Th species are shown by dashed and solid lines, respectively. The calculations of phase equilibria are based on thermodynamic data from *Barin* [1995].

[27] The NVP are observed to have lower Mg/Si values than surrounding terrain (Table 1), implying a lower degree of mantle melting in the magma source regions and lower S contents. In contrast, the possibly higher degrees of melting in the source regions of the IcP-HCT materials are apparently associated with more S-rich melts. Therefore, Mercury's mantle could be rich in sulfides, and undersaturation of magma with respect to S may play a lesser role on variable S abundances than does the fO_2 in mantle source regions and/or assimilated crustal materials.

[28] The temperature of Mercury's subsurface allows preservation of native S [*Vasavada et al*., 1999] formed through condensation of volcanic S_2 gas. Assimilation of condensed native sulfur (S_8) by hot crustal magmas could partially oxidize sulfide sulfur (S^{2-}) and other elements (e.g., N, C) in the melts. The corresponding decreases in solubilities will cause degassing of S_2, N_2, CO, and COS, leading to pyroclastic activity [cf. *Zolotov*, 2011], as observed in some regions [*Kerber et al*., 2011]. Interaction of upwelling magmas with native S deposits in the crust could be a major contributor to pyroclastic activity. However, the low fS_2 in equilibrium with Fe, Mg, Mn, and Ca sulfides implies only minor S_2 degassing from melts that avoided assimilation of crustal S and/or oxidation. The generally effusive nature of most volcanism on Mercury [*Head et al*., 2009] and the rarity of shallow magma chambers [*Head et al*., 2012] are consistent with limited degassing, condensation, assimilation, and volcanic recycling of S. It also follows that S_2 degassing did not have a strong effect on reduction of melts remaining in magma chambers and lava flows.

[29] The reducing conditions should have affected partitioning of elements between silicate, metal, and sulfide phases during core formation, at any magma ocean stage, and during subsequent magmatism [e.g., *Righter*, 2003; *Jurewicz et al*., 1995; *O'Neill and Eggins*, 2002; *Malavergne et al*., 2007b, 2010; *Wade et al*., 2012; *McCubbin et al*., 2012]. Although U and Th become increasingly chalcophile and siderophile at $fO_2 <$ IW, sulfidation of Th oxides occurs at lower fO_2 than U [*Malavergne et al*., 2010; *Sato and Kirishima*, 2010] (Figure 6). The Th/U ratio in Mercury's surface materials (2.5 ± 0.9) is only slightly less than in planetary and chondritic materials [*Peplowski et al*., 2011] and indicates differentiation outside the fO_2 range at which U and Th separate. A major sequestration of U and Th in the core at extremely reducing conditions ($fO_2 <$ 8.5-IW, Figure 6) may not be consistent with relatively high surface abundances of U and Th, which are comparable with concentrations in terrestrial oceanic crust and Martian basalts [*Peplowski et al*., 2011, 2012]. Therefore, conditions during differentiation could not have been more reduced than ~IW-6 ± 0.5 (*Malavergne et al*., 2007b, Figure 6). Uranium and Th should not separate at more oxidizing conditions. Note that the Th/U ratio in Mercury materials is also in disagreement with an explanation for the high K/Th ratio (8000 ± 3200 [*Peplowski et al*., 2012]) involving a strong partition of Th into core sulfides as discussed by *McCubbin et al*. [2012]. High-pressure experimental data on the sulfide-oxide partitioning behavior for Th would further constrain redox conditions at the time of core formation [*McCubbin et al*., 2012]. The possible redistribution of K in surface materials by thermal or other surface processes should be taken into account in the interpretation of the K/Th ratio [*Peplowski et al*., 2012].

[30] The high S contents in surface materials and the corresponding low fO_2 in magmas imply that Mercury accreted from reduced materials (FeO-poor silicates, Mg and Ca sulfides, Si-rich Fe-Ni metal) broadly similar to the constituents in enstatite chondrites [*Nittler et al*., 2011]. Although enstatite chondrites are thought to have formed sunward of the asteroid belt [at ~1–1.4 AU; *Wasson*, 1988; *Shukolyukov and Lugmair*, 2004; *Lee et al*., 2009; *Javoy et al*., 2010], Mercury-forming solids would likely have originated closer to the Sun [*O'Brien et al*., 2006; *Ebel and Alexander*, 2011]. It follows that Mercury's initial materials could be more reduced and depleted in FeS than enstatite chondrites due to incongruent evaporation of troilite in the hot inner nebula [*Tachibana and Tsuchiyama*, 1998]. Enstatite chondrites have the lowest Mg/Si ratio among chondrite groups, and an even lower Mg/Si ratio may be expected on Mercury (though the surface composition may not reflect the bulk ratio because of magmatic processes and Si in the core). For example, sulfidation of Mg and Ca silicates by S-rich gas released from Fe-FeS melts in the early inner solar system would lead to temperature-resistant Ca and Mg sulfides and also may result in the loss of Mg gas [*Lehner et al*., 2013]. Fe metal left after evaporation of S from the Fe-FeS melt might have contributed to Mercury's unusually high bulk density.

[31] Although a low FeS/(CaS + MgS + Fe) ratio in materials accreted by Mercury is consistent with the measured surface composition, such a ratio needs to be reconciled with the possible presence of a dense solid layer beneath the silicate mantle that could be rich in FeS and/or FeO [*Smith et al*., 2012]. At the lowest fO_2 values inferred here, Fe-Si core compositions could be more favorable than an Fe-S-Si composition [e.g., *Berthet et al*., 2009]. The Fe-Si compositional end-member does not exhibit the liquid-liquid immiscibility that could segregate a liquid FeS layer at the top of the core that may later have (partially) solidified.

[32] Despite a major sequestration of Fe-FeS melts into the core, dissolved sulfur should have remained abundant in reduced silicate melts during and after differentiation (e.g., in a magma ocean). The dominance of silicates at the surface of Mercury is not consistent with the large-scale separation of low-density Ca and Mg sulfides by flotation in silicate magma. This inference is consistent with the lower crystallization temperature of sulfides than of Mg silicates and sulfide melt separation only at a small length scales [*McCoy et al*., 1999]. In other words, because

sulfides crystallize after substantial crystallization of silicates, they may not float in high viscosity, crystal-rich magma despite their buoyancy. The likely presence of Fe in Mg- and/or Ca-rich sulfide melts increases their density and further restricts their buoyancy. In contrast to immiscible FeS-rich melts, Mg-Ca-Fe-sulfide melts should not sink in magma chambers or thick lava flows. Therefore, S concentration in surface materials may represent S dissolved within the silicate melt at the time of partial melting (except in cases when crustal S is assimilated). We conclude that the high S solubility in reduced melts can account for the observations without major sulfide separation through flotation. It follows that Ca, Mg, and Fe sulfides were imbedded in the initial solidified mantle. Subsequent partial melting of the mantle would have mobilized sulfur into silicate melts that eventually erupted at the surface, where sulfides crystallized later than major silicate phases.

4. Concluding Remarks

[33] The elevated concentrations of S in surface materials on Mercury, along with low FeO content in surface silicates, indicate that the magmas that formed volcanic rocks on Mercury were strongly reduced. Both upper limits on the FeO content and the high S concentrations in surface materials have been used to evaluate fO_2 in magmas. The fO_2 values estimated from Mg silicate-sulfide equilibrium and sulfide capacity data on metallurgical slags lead to similar results. The average fO_2 in magmas on Mercury is estimated to lie between ~5 and ~6.5 log units below the iron-wüstite buffer. This fO_2 range corresponds to FeO concentrations of 0.07–0.44 wt %, which are markedly less than upper limits obtained from spectral reflectance measurements. Spatial variations of fO_2 could be between IW-7.3 and IW-4.5, possibly reflecting differences in the S abundance and the silicate composition. Mercury's northern volcanic plains could be slightly more reduced than surrounding regions, although the difference is not statistically significant. The evaluated fO_2 values and FeO contents in volcanic rocks are consistent with the presence of Mg and/or Ca sulfides together with troilite and Fe^0-metal as products of the crystallization of erupted lavas, but ilmenite is excluded by this argument.

[34] The fO_2 values of ~5–7 log units below the IW buffer are similar to fO_2 values estimated for the canonical solar nebula [e.g., *Grossman et al*., 2008; *Lehner et al*., 2013; *Jurewicz et al*., 1995]. It is likely, therefore, that Mercury's precursory materials were not oxidized in the inner solar nebula, in contrast to those from which the asteroids and other terrestrial planets formed (except for the parent bodies of enstatite chondrites).

[35] The Th/U ratio in surface materials is not much different from that on other solid planetary bodies [*Peplowski et al*., 2011] and could be inconsistent with $fO_2 < \text{IW-6} \pm 0.5$, at which Th and U may separate during differentiation. Experiments on fO_2-dependent sulfide-silicate fractionation of Th will further constrain fO_2 on Mercury.

[36] The fO_2 values obtained from Mercury's S contents and slag-based sulfide capacity data are lower than estimates derived from petrologic experiments that provide data on S solubility in Fe^0-saturated melts. The discrepancy may reflect the inapplicability of slag models to magma compositions on Mercury, uncertain values of fS_2 in petrologic experiments, and/or other factors. Therefore, we encourage experimental investigations of sulfide-silicate melt partitioning of S at controlled fS_2 and fO_2 to obtain sulfide capacity data for magma compositions directly relevant to conditions on Mercury. Further evaluation of igneous systems on Mercury will also depend on understanding the scale of surface processes that modify volcanic rocks and redistribute volatile species.

[37] **Acknowledgments.** The MESSENGER project is supported by the NASA Discovery Program under contracts NAS5-97271 to The Johns Hopkins University Applied Physics Laboratory and NASW-00002 to the Carnegie Institution of Washington. The work of M.Z. is supported by grants from the NASA Cosmochemistry and Planetary Geology and Geophysics programs and the NSF Planetary Astronomy program. This paper has benefited from the ideas of Michael Petaev about the role of Fe-FeS equilibrium, as well as comments from Alexander Borisov, Francis McCubbin, Seshadri Seetharaman, Stephen Lehner, and William Vaughan.

References

Ariskin, A. A., A. A. Borisov, and G. S. Barmina (1993), Simulating iron-silicate melt equilibrium in basaltic systems, *Geochem. Int.*, *30*, 13–22.

Barin, I. (1995), Thermochemical Data of Pure Substances, 3rd ed., VCH, Weinheim.

Bekker, A., M. E. Barley, M. L. Fiorentini, O. J. Rouxel, D. Rumble, and S. W. Beresford (2009), Atmospheric sulfur in Archean komatiite-hosted nickel deposits, *Science*, *326*, 1086–1089.

Berthet, S., V. Malavergne, and K. Righter (2009), Melting of the Indarch meteorite (EH4 chondrite) at 1 GPa and variable oxygen fugacity: Implications for early planetary differentiation processes, *Geochim. Cosmochim. Acta*, *73*, 6402–6420.

Blewett, D. T., P. G. Lucey, B. R. Hawke, G. G. Ling, and M. S. Robinson (1997), A comparison of mercurian reflectance and spectral quantities with those of the Moon, *Icarus*, *129*, 217–231.

Blewett, D. T., et al. (2013), Mercury's hollows: Constraints on formation and composition from analysis of geological setting and spectral reflectance, *J. Geophys. Res.*, *118*, doi:10.1029/2012JE004174.

Brearley, A. J., and R. H. Jones (1998), Chondritic meteorites, in *Planetary Materials*, edited by J. J. Papike, *Rev. Mineral*., *36*, pp. 1–398, Mineral. Soc. Am., Washington, D.C.

Boynton, W. V., A. L. Sprague, S. C. Solomon, R. D. Starr, L. G. Evans, W. C. Feldman, J. I. Trombka, and E. A. Rhodes (2007), MESSENGER and the chemistry of Mercury's surface, *Space Sci. Rev.*, *131*, 85–104.

Burbine, T. H., T. J. McCoy, L.R. Nittler, G. K. Benedix, E. A. Cloutis, and T. L. Dickinson (2002), Spectra of extremely reduced assemblages: Implications for Mercury, *Meteorit. Planet. Sci.*, *37*, 1233–1244.

Denevi, B. W., and M. S. Robinson (2008), Mercury's albedo from Mariner 10: Implications for the presence of ferrous iron, *Icarus*, *197*, 239–246.

Duffy, J. A. (1996), Optical basicity: A practical acid-base theory for oxides and oxyanions, *J. Chem. Educ.*, *73*, 1138–1142.

Ebel, D. S., and C. M. O'D. Alexander (2011), Equilibrium condensation from chondritic porous IDP enriched vapor: Implications for Mercury and enstatite chondrite origins, *Planet. Space Sci.*, *59*, 1888–1894.

Evans, L. G., et al. (2012), Major-element abundances on the surface of Mercury: Results from the MESSENGER Gamma-Ray Spectrometer, *J. Geophys. Res.*, *117*, E00L07, doi:10.1029/2012JE004178.

Fogel, R. A., M. K. Weisberg, and M. Prinz (1996), The solubility of CaS in aubrite silicate melts, *Lunar Planet. Sci.*, *27*, 371–372.

Grossman, L., J. R. Beckett, A. V. Fedkin, S. B. Simon, and F. J. Ciesla (2008), Redox conditions in the solar nebula: Observational, experimental, and theoretical constraints, in *Oxygen in the Solar System*, edited by G. J. MacPherson, D. W. Mittlefehldt, J. H. Jones, and S. B. Simon, pp. 93–140, Mineral. Soc. of America. Chantilly, Virginia.

Guillermet, A. F., M. Hillert, B. Jansson, and B. Sundman (1981), An assessment of the Fe-S system using a 2-sublattice model for the liquid-phase, *Metall. Mater. Trans. B*, *12*, 745–754.

Head, J. W., et al. (2009), Volcanism on Mercury: Evidence from the first MESSENGER flyby for extrusive and explosive activity and the volcanic origin of plains, *Earth Planet. Sci. Lett.*, *285*, 227–242.

Head, J. W., et al. (2012), Effusive volcanism on Mercury from MESSENGER mission data: Nature and significance for lithospheric stress and mantle convection, *Lunar Planet. Sci.*, *43*, abstract 1451.

Javoy, M., et al. (2010), The chemical composition of the Earth: Enstatite chondrite models, *Earth Planet. Sci. Lett.*, *293*, 259–268.

Jurewicz, S. R., J. H. Jones, and B. Fegley Jr. (1995), Experimental partitioning of Zr, Nb, and Ti between platinum group metals and silicate liquid:

Implications for the origin of refractory metal nuggets in carbonaceous chondrites, *Earth Planet. Sci. Lett.*, *132*, 183–198.
Keil, K. (1968), Mineralogical and chemical relationships among enstatite chondrites, *J. Geophys. Res.*, *73*, 6945–6976.
Kerber, L., J. W. Head, S. C. Solomon, L. Wilson, S. L. Murchie, M. S. Robinson, B. W. Denevi, and D. L. Domingue (2011), The global distribution of pyroclastic deposits on Mercury: The view from MESSENGER flybys 1–3, *Planet. Space Sci.*, *59*, 1895–1909.
Lee, J.-Y., K. Marti, and J. F. Wacker (2009), Xe isotopic abundances in enstatite meteorites and relations to other planetary reservoirs, *J. Geophys. Res.*, *114*, E04003, doi:10.1029/2008JE003082.
Lehner, S. W., M. I. Petaev, M. Yu. Zolotov, and P. R. Buseck (2013), Formation of niningerite by silicate sulfidation in EH3 enstatite chondrites, *Geochim. Cosmochim. Acta*, *101*, 34–56.
Liu, S-H, R. J. Fruehan, A. Morales, and B. Ozturk (2001), Measurement of FeO activity and solubility of MgO in smelting slags, *Metall. Mater. Trans. B*, *32B*, 31–36.
Malavergne, V., S. Berthet, and K. Righter, (2007a), Formation of CaS-MgS in enstatite chondrites and achondrites as a function of redox conditions and temperature: Constraints on their evolution in a planetesimal and in a proto-planet, *Lunar Planet. Sci.*, *38*, abstract 1737.
Malavergne, V., M. Tarrida, R. Combes, H. Bureau, J. Jones, and C. Schwandt (2007b), New high-pressure and high-temperature metal/silicate partitioning of U and Pb: Implications for the cores of the Earth and Mars, *Geochim. Cosmochim. Acta*, *71*, 2635–2655.
Malavergne, V., M. J. Toplis, S. Berthet, and J. Jones (2010), Highly reducing conditions during core formation on Mercury: Implications for internal structure and the origin of a magnetic field, *Icarus*, *206*, 199–209.
Malavergne, V., F. Brunet, K. Righter, B. Zanda, C. Avril, S. Borensztajn, and S. Berthet (2012), Experimental behavior of sulfur under primitive planetary differentiation processes, the sulfide formations in enstatite meteorites and implications for Mercury, *Lunar Planet. Sci.*, *43*, abstract 1860.
McClintock, W. E., et al. (2008), Spectroscopic observations of Mercury's surface reflectance during MESSENGER's first Mercury flyby, *Science*, *321*, 62–65.
McCoy, T. J., T. L. Dickinson, and G. E. Lofgren (1999), Partial melting of the Indarch (EH4) meteorite: A textural, chemical, and phase relations view of melting and melt migration, *Meteorit. Planet. Sci.*, *34*, 735–746.
McCubbin, F. M., M. A. Riner, K. E. Vander Kaaden, and L. K. Burkemper (2012), Is Mercury a volatile-rich planet?, *Geophys. Res. Lett.*, *39*, L09202, doi:10.1029/2012GL051711.
Nittler, L. R., et al. (2011), The major-element composition of Mercury's surface from MESSENGER X-ray spectrometry, *Science*, *333*, 1847–1850.
Nzotta, M. M., D. Sichen, and S. Seetharaman (1999), Study of the sulfide capacities of iron-oxide containing slags, *Metall. Mater. Trans. B*, *30B*, 909–919.
O'Brien, D. P., A. Morbidelli, and H. F. Levison (2006), Terrestrial planet formation with strong dynamical friction, *Icarus*, *184*, 39–58.
O'Neill, H. St. C., and S. M. Eggins (2002), The effect of melt composition on trace element partitioning: An experimental investigation of the activity coefficients of FeO, NiO, CoO, MoO_2 and MoO_3 in silicate melts, *Chem. Geol.*, *186*, 151–181.
Pankratz, L. B., A. D. Mah, and S. W. Watson (1987), Thermodynamic Properties of Sulfides, Bureau of Mines Bulletin 689, 427 pp., U.S. Department of the Interior, Washington, D.C.
Peplowski, P. N., et al. (2011), Radioactive elements on Mercury's surface from MESSENGER: Implications for the planet's formation and evolution, *Science*, *333*, 1850–1852.
Peplowski, P. N., et al. (2012), Variations in the abundances of potassium and thorium on the surface of Mercury: Results from the MESSENGER Gamma-Ray Spectrometer, *J. Geophys. Res.*, *117*, E00L04, doi:10.1029/2012JE004141.
Richardson, F. D., and C. J. B. Fincham (1954), Sulfur in silicate and aluminate slags, *J. Iron. Steel Res. Int.*, *178*, 4–15.
Righter, K. (2003), Metal-silicate partitioning of siderophile elements and core formation in the early Earth, *Annu. Rev. Earth Planet. Sci.*, *31*, 135–174.
Riner, M. A., F. M. McCubbin, P. G. Lucey, G. J. Taylor, and J. J. Gillis-Davis (2010), Mercury surface composition: Integrating petrologic modeling and remote sensing data to place constraints on FeO abundance, *Icarus*, *209*, 301–313.
Robie, R. A., and B. S. Hemingway (1995), Thermodynamic Properties of Minerals and Related Substances at 298.15 K and 1 Bar (10^5 Pascals) Pressure and at Higher Temperatures, U.S. Geological Survey Bull. 2131, U.S. Department of the Interior, Washington, D.C.
Robinson, M. S., and G. J. Taylor (2001), Ferrous oxide in Mercury's crust and mantle, *Meteorit. Planet. Sci.*, *36*, 841–847.
Roeder, P. L. (1974), Activity of iron and olivine solubility in basaltic liquids, *Earth Planet. Sci. Lett.*, *23*, 397–410.
Sato, N., and A. Kirishima (2010), Separation of thorium and uranium by sulfide method, *Energy Procedia*, *7*, 444–448.
Shankar, A., M. Görnerup, A. K. Lahiri, and S. Seetharaman (2006), Sulfide capacity of high alumina blast furnace slags, *Metall. Mater. Trans. B*, *37B*, 941–947.
Shukolyukov, A., and G. W. Lugmair (2004), Manganese-chromium isotope systematic of enstatite meteorites, *Geochim. Cosmochim. Acta*, *68*, 2875–2888.
Smith, D. E., et al. (2012), Gravity field and internal structure of Mercury from MESSENGER, *Science*, *336*, 214–217.
Sosinsky, D. J., and I. D. Sommerville (1986), The composition and temperature dependence of the sulfide capacity of metallurgical slags, *Metall. Mater. Trans. B*, *17B*, 331–337.
Sprague, A. L., K. L. Donaldson Hanna, R. W. H. Kozlowski, J. Helbert, A. Maturilli, J. B. Warell, and J. L. Hora (2009), Spectral emissivity measurements of Mercury's surface indicate Mg- and Ca-rich mineralogy, K-spar, Na-rich plagioclase, rutile, with possible perovskite, and garnet, *Planet. Space Sci.*, *57*, 364–383.
Sprague, A. L., D. M. Hunten, and K. Lodders (1995), Sulfur at Mercury, elemental at the poles and sulfides in the regolith, *Icarus*, *118*, 211–215.
Starr, R. D., D. Schriver, L. R. Nittler, S. Z. Weider, P. K. Byrne, G. C. Ho, E. A. Rhodes, C. E. Schlemm, II, S. C. Solomon, and P. M. Trávníček (2012), MESSENGER detection of electron-induced X-ray fluorescence from Mercury's surface, *J. Geophys. Res.*, *117*, E00L02, doi:10.1029/2012JE004118.
Stockstill-Cahill, K. R., T. J. McCoy, L. R. Nittler, S. Z. Weider, and S. A. Hauck II (2012), Magnesium-rich crustal compositions on Mercury: Implications for magmatism from petrologic modeling, *J. Geophys. Res.*, *117*, E00L15, doi:10.1029/2012JE004140.
Tachibana, S., and A. Tsuchiyama (1998), Incongruent evaporation of troilite (FeS) in the primordial solar nebula: An experimental study, *Geochim. Cosmochim. Acta*, *62*, 2005–2022.
Taniguchi, Y., N. Sano, and S. Seetharaman (2009), Sulphide capacities of CaO-Al_2O_3-SiO_2-MgO-MnO slags in the temperature range 1673-1773 K, *ISIJ Int.*, *49*, 156–163.
Taylor, G. J., and E. R. D. Scott (2003), Mercury, in *Meteorites, Comets and Planets*, edited by A. M. Davis, Treatise on Geochemistry, vol. 1, pp. 477–485, Elsevier, Pergamon, Oxford, U.K.
Vasavada, A. R., D. A. Page, and S. E. Wood (1999), Near-surface temperatures on Mercury and the Moon and the stability of polar ice deposits, *Icarus*, *141*, 179–193.
Vernazza, P., F. DeMeo, D. A. Nedelcu, M. Birlan, A. Doressoundiram, S. Erard, and E. Volquardsen (2010), Resolved spectroscopy of Mercury in the near-IR with SpeX/IRTF, *Icarus*, *209*, 125–137.
Vilas, F. (1988), Surface composition of Mercury from reflectance spectrophotometry, in Mercury, edited by F. Vilas, C. R. Chapman, and M. S. Matthews, pp. 59–76, University of Arizona Press, Tucson, Ariz.
Vilas, F., D. L. Domingue, A. L. Sprague, N. R. Izenberg, R. L. Klima, E. A. Jensen, J. Helbert, M. D'Amore, K. R. Stockstill-Cahill, and S. C. Solomon (2012), Search for absorption features in Mercury's visible reflectance spectra: Recent results from MESSENGER, *Lunar Planet. Sci.*, *43*, abstract 1330.
Wade, J., B. J. Wood, and J. Tuff (2012), Metal-silicate partitioning of Mo and W at high pressures and temperatures: Evidence for late accretion of sulphur to the Earth, *Geochim. Cosmochim. Acta*, *85*, 58–74.
Wasson, J. T. (1988), The building stones of the planets, in Mercury, edited by F. Vilas, C. R. Chapman, and M. S. Matthews, pp. 622–650, University of Arizona Press, Tucson, Ariz.
Weider, S. Z., L. R. Nittler, R. D. Starr, T. J. McCoy, K. R. Stockstill-Cahill, P. K. Byrne, B. W. Denevi, J. W. Head, and S. C. Solomon (2012), Compositional heterogeneity on Mercury's surface revealed by the MESSENGER X-Ray spectrometer, *J. Geophys. Res.*, *117*, E00L05, doi:10.1029/2012JE004153.
Weider, S. Z., L. R. Nittler, R. D. Starr, and S. C. Solomon (2012), The distribution of iron on the surface of Mercury from MESSENGER X-Ray Spectrometer measurements, *Lunar Planet. Sci.*, *44*, abstract 2189.
Young, R. W., J. A. Duffy, G. J. Hussall, and Z. Hu (1992), Use of optical basicity concept for determining phosphorous and sulfur slag-metal partitions. *Ironmaking Steelmaking*, *19*, 201–219.
Zolotov, M. Yu. (2011), On the chemistry of mantle and magmatic volatiles on Mercury, *Icarus*, *212*, 24–41.